BIOCHEMISTRY
including biophysical chemistry & molecular biology
Article

Biochemistry **2010,** *49,* 9551–9562 9551
DOI: 10.1021/bi101245j

Myristate Exposure in the Human Immunodeficiency Virus Type 1 Matrix Protein Is Modulated by pH[†]

Emily L. Fledderman,[‡] Ken Fujii,[§] Ruba H. Ghanam,[‡] Kayoko Waki,[§] Peter E. Prevelige,[‡] Eric O. Freed,[§] and Jamil S. Saad*,[‡]

[‡]*Department of Microbiology, University of Alabama at Birmingham, Birmingham, Alabama 35294, United States, and* [§]*Virus-Cell Interaction Section, HIV Drug Resistance Program, National Cancer Institute at Frederick, Frederick, Maryland 21702, United States*

Received August 4, 2010; Revised Manuscript Received September 29, 2010

ABSTRACT: Human immunodeficiency virus type 1 (HIV-1) encodes a polypeptide called Gag that is capable of forming virus-like particles (VLPs) in vitro in the absence of other cellular or viral constituents. During the late phase of HIV-1 infection, Gag polyproteins are transported to the plasma membrane (PM) for assembly. A combination of in vivo, in vitro, and structural studies have shown that Gag targeting and assembly on the PM are mediated by specific interactions between the myristoylated matrix [myr(+)MA] domain of Gag and phosphatidylinositol 4,5-bisphosphate [PI(4,5)P_2]. Exposure of the MA myristyl (myr) group is triggered by PI(4,5)P_2 binding and is enhanced by factors that promote protein self-association. In the studies reported here, we demonstrate that myr exposure in MA is modulated by pH. Our data show that deprotonation of the His89 imidazole ring in myr(+)MA destabilizes the salt bridge formed between His89(Hδ2) and Glu12 (COO-), leading to tight sequestration of the myr group and a shift in the equilibrium from trimer to monomer. Furthermore, we show that oligomerization of a Gag-like construct containing matrix-capsid is also pH-dependent. Disruption of the His−Glu salt bridge by single-amino acid substitutions greatly altered the myr-sequestered−myr-exposed equilibrium. In vivo intracellular localization data revealed that the H89G mutation retargets Gag to intracellular compartments and severely inhibits virus production. Our findings reveal that the MA domain acts as a "pH sensor" in vitro, suggesting that the effect of pH on HIV-1 Gag targeting and binding to the PM warrants investigation.

Retroviral genomes encode a polyprotein called Gag that contains all the viral elements required for virus assembly and is capable of forming virus-like particles (VLPs) in vitro in the absence of viral and cellular constituents (*1*, *2*). Subsequent to their synthesis, Gag polyproteins are transported to the plasma membrane (PM) for assembly and budding (*3*−*6*). During or shortly after budding, the Gag proteins are cleaved by the viral protease into matrix (MA), capsid (CA), nucleocapsid (NC), and short peptides (SP1, SP2, and P6), which rearrange to form mature and infectious virions (*4*−*6*).

It is widely accepted that HIV-1[1] Gag budding and assembly occur predominantly on the PM (*6*−*15*). Membrane binding is mediated by Gag's N-terminal myristoylated MA domain [myr(+)MA]. The myristyl group (myr) functions in concert with a group of conserved basic residues to facilitate membrane anchoring and assembly of Gag (*4*−*6*). Mutations that either block myristoylation or disrupt the basic patch lead to inefficient targeting of Gag to the PM, resulting in a dramatically reduced level of virus production (*9*, *16*−*19*).

NMR-based structural studies confirmed that the myr group of HIV-1 MA can adopt sequestered [myr(s)] and exposed [myr(e)] conformations (*20*). The extent of extrusion of the myr group can be increased by factors that promote protein self-association, such as increasing protein concentration or inclusion of the CA domain (*20*). Equilibrium data revealed that while myr(+)MA resides in a monomer−trimer equilibrium, the myr(−)MA protein maintains its monomeric character in solution under all conditions (*20*). In addition, exposure of the myr group is coupled with protein trimerization (*20*). Despite a high degree of sequence and structural homology, we have recently shown that factors affecting the myr switch mechanism are significantly different for the HIV-1 and HIV-2 MA proteins (*21*). Structural studies on HIV-2 MA revealed that the myr group is tightly sequestered and the protein is in the monomeric state, indicating that key differences in the myr switch mechanism can exist between closely related retroviruses (*21*).

Studies by Freed, Ono, and co-workers demonstrated that the ultimate localization of HIV-1 Gag at virus assembly sites is dependent on phosphatidylinositol 4,5-bisphosphate [PI(4,5)P_2] (*22*−*24*), a cellular factor localized at the inner leaflet of the PM (*25*−*27*). Subsequent structural studies revealed that PI(4,5)P_2 binds directly to HIV-1 MA, inducing a conformational change that triggers myr exposure (*28*). On the other hand, although HIV-2 Gag localization on the PM is also dependent on

[†]This work was supported by the UAB Comprehensive Cancer Center (National Cancer Institute Grant P30CA13148) to J.S.S., the Intramural Research Program of the Center for Cancer Research (National Cancer Institute), and the Intramural AIDS Targeted Antiviral Program (to E.O.F.).

*To whom correspondence should be addressed: 845 19th St. S., Birmingham, AL 35294. Phone: (205) 996-9282. Fax: (205) 996-4008. E-mail: saad@uab.edu.

[1]Abbreviations: HIV-1, human immunodeficiency virus type 1; HIV-1 MA, HIV-1 matrix protein; HIV-1 Gag, myristoylated HIV-1 Gag polyprotein; myr(−), unmyristoylated protein; myr(+), myristoylated protein; CA, capsid; MACA, matrix-capsid; MVB, multivesicular body; PI(4,5)P_2, phosphatidylinositol 4,5-bisphosphate; NMR, nuclear magnetic resonance; SV, sedimentation velocity; SE, sedimentation equilibrium.

Published on Web 10/01/2010

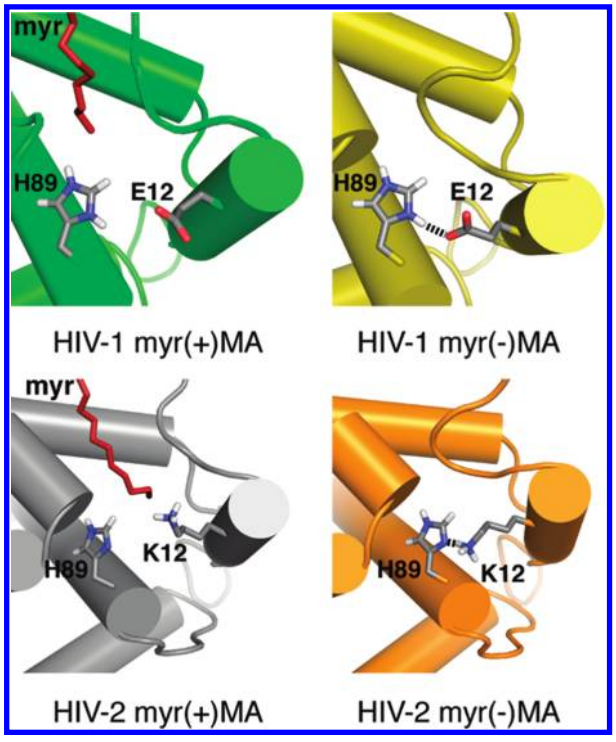

FIGURE 1: Comparison of HIV-1 and HIV-2 MA protein structures. The imidazole ring of His89 forms a salt bridge with Glu12(COO-) in HIV-1 myr(−)MA but not in the myr(+)MA protein. For HIV-2, Glu12 is substituted with Lys, which can form a hydrogen bond with deprotonated His89 in myr(−)MA.

$PI(4,5)P_2$, structural studies have shown that the myr switch of HIV-2 MA is less sensitive to $PI(4,5)P_2$ binding than that of HIV-1 (*21*).

To dissect the underlying differences in the myr switch mechanism in HIV-1 and HIV-2 MA proteins, we focused on some key differences in the N-terminal domain, including the first 20 residues. We observed that Glu12 in HIV-1 MA is substituted with Lys in HIV-2 MA (*21*). Analysis of the HIV-1 myr(+)MA structure revealed that the imidazole ring of His89, which is highly conserved among all strains of HIV-1, HIV-2, and simian immunodeficiency virus (SIV) (Los Alamos National Laboratory, http://www.hiv.lanl.gov), forms a salt bridge with Glu12(COO-) in HIV-1 myr(−)MA but not in the myr(+)MA protein (Figure 1).

Histidines are central in biological activities because of their frequent inclusion in the active sites of enzymes and their contributions to protein stability and function. The intrinsic pK_a of the histidine imidazole group typically lies between 6.0 and 7.0 (*29*, *30*) but can vary depending on the degree of burial or exposure within proteins (*30*). Earlier studies have shown that mutation of His89 and other residues in the vicinity led to targeting of Gag to intracellular compartments and severely reduced virus production (*18*). These findings, combined with our recent structural studies, indicate that His89 may play a central role in determining the site of Gag assembly and ultimately efficient virus production.

We have employed NMR, biophysical techniques, mutagenesis, and in vivo studies to identify the precise functional role of the His89−Glu12 salt bridge in regulating the myr switch mechanism, HIV-1 Gag targeting, and virus replication. Our results demonstrate that extrusion of the myr group in the HIV-1 MA protein is sensitive to changes in pH. In vivo intracellular localization data revealed that H89G mutation retargets Gag to intracellular compartments and severely inhibits virus production.

EXPERIMENTAL PROCEDURES

Sample Preparation. A co-expression vector encoding the HIV-1 MA gene and a yeast *N*-myristyltransferase (yNMT) was kindly provided by M. Summers (Howard Hughes Medical Institute, University of Maryland, Baltimore County, Baltimore, MD). To construct the MACA clone, the MACA coding sequence was PCR-amplified from the pNL4-3 isolate (NCBI accession code M15390) and cloned into the co-expression vector described above at its NcoI and XhoI sites in frame with the C-terminal His_6 tag and stop codon of the plasmid. An expression vector encoding the HIV-1 CA domain was kindly provided by P. Prevelige [University of Alabama at Birmingham (UAB)]. A QuickChange XL site-directed mutagenesis kit (Stratagene, La Jolla, CA) was used to generate a subset of MA and MACA mutants (MA-H89G, MA-E12A, MACA-W184A/M185A, and MACA-E12A/W184A/M185A). Mutations were verified by plasmid sequencing at the Center for AIDS Research core facility (UAB).

Preparation of MA, CA, and MACA protein samples has been described elsewhere (*20*, *28*, *31*−*33*). Mutant MA samples were prepared like wild-type (WT) MA. However, although the myr(−)MA H89G protein was very soluble, the myr(+)MA H89G protein was found exclusively in the pellet, purified under denaturing conditions (8 M urea), and refolded through extensive stepwise dialysis. Because of protein precipitation, myr(+)MA H89G samples were kept at concentrations lower than ~40 μM. Molecular masses of proteins and the efficiency of myristoylation were confirmed by electrospray ionization mass spectrometry. Samples for all NMR experiments were prepared in 50 mM sodium phosphate, 100 mM NaCl, and 2 mM DTT. NMR sample concentrations of MA proteins varied from 50 to 700 μM.

NMR Spectroscopy. NMR data were collected on a Bruker Avance II (700 MHz ^{1}H) spectrometer equipped with a cryoprobe, processed with NMRPIPE (*34*), and analyzed with NMRVIEW (*35*). Two- and three-dimensional (2D and 3D, respectively) NOESY data were obtained for natural abundance, ^{15}N-labeled, and ^{15}N- and ^{13}C-labeled protein samples (pH 7.2, 35 °C). Protein signal assignments were described elsewhere (*20*, *28*, *31*, *32*). ^{1}H−^{1}H NOEs between the ^{15}N- and ^{13}C-labeled protein and the unlabeled myristate group were assigned from 2D (^{1}H−^{1}H) and 3D (^{13}C- and ^{13}C-edited/^{12}C-double-half-filtered) NOESY data (see ref *36* and *37* and references cited therein).

Determination of the His89 pK_a Value. The pK_a value of His89 for myr(−)MA and myr(+)MA proteins was calculated on the basis of the pH-dependent His Hε1 and Cε1 chemical shifts extracted from the 2D HMQC (heteronuclear multiple-quantum coherence) data. Protein concentrations were 150 μM. The sample pH was adjusted to the desired value with DCl or NaOD. pH values were measured at room temperature before and after the collection of NMR data. The values were not corrected for the deuterium isotope effect. NMR spectra were recorded between pH 4.2 and 8.8. No chemical shift changes occurred below pH 4.2 or above pH 8.8. The pH titration curves were fitted to a modified Henderson−Hasselbalch equation by nonlinear least-squares analysis:

$$\delta_{obs} = (\delta_{acid} + \delta_{base} \times 10^{pH - pK_a})/(1 + \delta_{base} \times 10^{pH - pK_a})$$

where δ_{obs} is the chemical shift observed at each pH value and δ_{acid} and δ_{base} are the chemical shift values for the protonated and deprotonated histidine, respectively. Curve fits were performed using ORIGIN version 8.1 (OriginLab, Northampton, MA).

Analytical Ultracentrifugation. Sedimentation velocity (SV) and sedimentation equilibrium (SE) measurements were taken with a Beckman XL-I Optima system equipped with a four-hole An-60 rotor (Beckman Coulter). Protein samples were prepared in 50 mM sodium phosphate buffer, 100 mM NaCl, and 2 mM tris(2-carboxyethyl)phosphine hydrochloride. Loading concentrations varied from 30 to 150 μM for MA and CA samples, while concentrations for MACA samples varied from 7 to 30 μM. The rotor speed for sedimentation velocity experiments was set at 40000 rpm, while sedimentation equilibrium data were collected at 22000, 26000, and 30000 rpm (20 °C). Scans were acquired at a wavelength of 280, 290, or 295 nm. Partial specific volumes (v-bar) and molar extinction coefficients were calculated using SEDNTERP, and buffer densities were measured pycnometrically. Sedimentation velocity data analysis were performed with SEDFIT (*38*, *39*), while sedimentation equilibrium data were analyzed with NONLIN (*40*) and HeteroAnalysis (J. L. Cole and J. W. Larry, Storrs, CT) (*41*). Sedimentation coefficients were corrected to 20 °C and infinite dilution in water, $s_{20,w}$. Equilibrium association constants were determined by global analysis of data acquired from samples prepared at three loading concentrations and centrifuged at three rotor speeds. Samples were sedimented at each velocity until equilibrium was achieved as judged by WinMatch (D. Yphantis, University of Connecticut, Storrs, CT, and J. Larry, National Analytical Ultracentrifugation Center, Storrs, CT).

CD Spectroscopy. CD spectra were recorded on a Jasco J815 spectropolarimeter at 25 °C from 260 to 185 nm. The scanning rate was set to 50 nm/min. Loading concentrations were 8 μM in buffer containing 50 mM sodium phosphate, 100 mM NaCl, and 2 mM tris(2-carboxyethyl)phosphine hydrochloride. The background signal from the buffer solution was subtracted from each spectrum.

Virus Replication. HIV-1 replication in T-cell lines was assessed via transfection of full-length pNL4-3 molecular clones (*42*) encoding WT or mutant MA domains by using the DEAE-dextran transfection methods (*18*). Cells were split 1:3 every two days, and virus replication was monitored by reverse transcriptase (RT) activity in the supernatant.

Gag Localization. Immunostaining of transfected HeLa cells was performed essentially as described previously (*19*, *43*). Gag localization was assessed by using a p17(MA)-specific monoclonal antibody (Advanced Biotechnologies, Columbia, MD). CD63 staining was performed with an antibody from Santa Cruz Biotechnology (Santa Cruz, CA). Images were acquired with a DeltaVision RT deconvolution microscope.

Nomenclature. In this study, MA mutants are named on the basis of the N-terminal Met, which is absent in the myristoylated protein, being designated as residue 1. In contrast, previous studies that included the initial characterization of the mutants investigated here (*18*, *43*−*45*) considered the N-terminal Gly of the myristoylated protein as residue 1. Thus, the mutant names are offset by one residue.

RESULTS

NMR pH Titrations of HIV-1 MA. It is well established that myristoylation of HIV-1 MA does not induce significant structural changes in the overall shape of the protein (*20*, *28*). However, significant NMR spectral and structural differences are evident for residues Ala3−Lys18 of myr(+)MA when compared to those of the myr(−)MA protein (*20*, *28*). These spectral differences reflect minor structural adjustments of the first loop

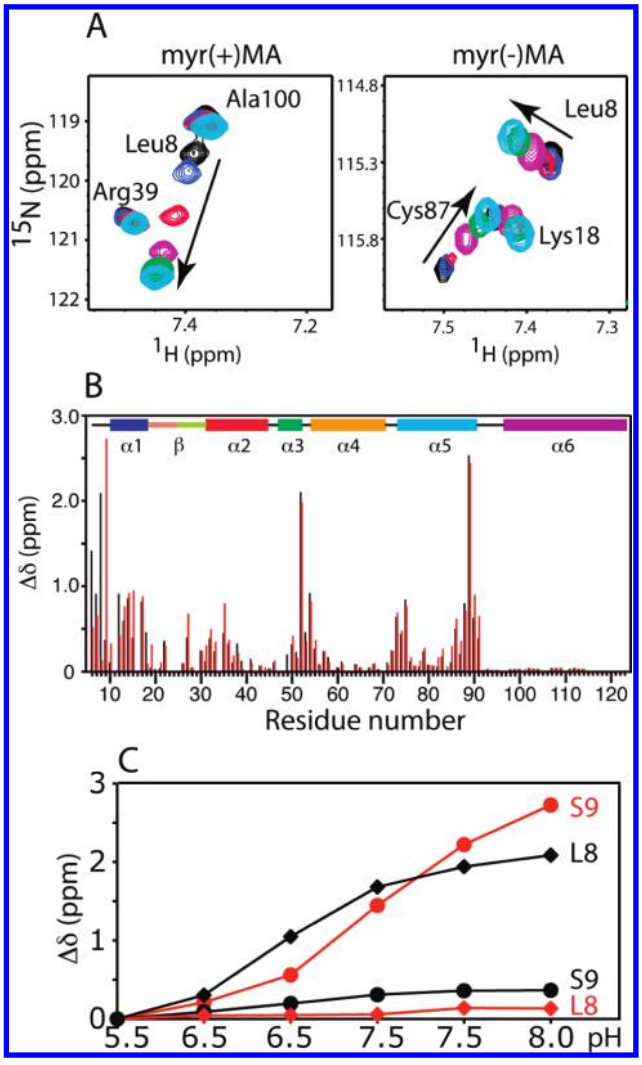

FIGURE 2: (A) Overlay of 2D ^{1}H−^{15}N HSQC spectra collected for HIV-1 myr(+)MA and myr(−)MA at pH 5.5 (black), 6.0 (blue), 6.5 (red), 7.0 (magenta), 7.5 (green), and 8.0 (cyan) (150 μM, 35 °C). (B) Histogram showing chemical shift changes extracted from the 2D HSQC data collected for myr(+)MA (black) and myr(−)MA (red) with an increase in the pH from 5.5 to 8.0. (C) Chemical shift changes for the ^{1}H−^{15}N resonances of Leu8 and Ser9 of myr(+)MA (black) and myr(−)MA (red).

(Ala3−Gly10) and helix I (Gly11−Lys18) to allow for sequestration of the myr group (*20*, *28*). The structure of the myr(−)MA protein is considered a representative model of myr(e)MA. One major difference between the structures of myr(+)MA and myr(−)MA proteins involves long-range interactions between the side chains of His89 and Glu12 (Figure 1). The carboxyl group of Glu12, which is located near the N-terminus of helix I, does not make long-range contacts in myr(+)MA but forms a salt bridge with His89(Hδ2) in myr(−)MA (*21*, *28*).

To test whether manipulation of the electronic properties of the imidazole group of His89 by changing the solution pH has an impact on the myr switch mechanism, we collected 2D ^{1}H−^{15}N HSQC NMR data for both myr(+)MA and myr(−)MA proteins with the pH increasing from 5.5 to 8.0 in 0.5 pH unit increments. As shown in Figure 2, substantial changes in the ^{1}H−^{15}N resonances $\{[(\Delta\delta^{1}\mathrm{H})^2 + (\Delta\delta^{15}\mathrm{N})^2]^{1/2} = 0.5-3.0$ ppm$\}$ were observed with a variation in pH (complete sets of HSQC data are shown in Figure S1 of the Supporting Information). These residues reside on the N-terminal loop (Ala3−Ser9) and helix I (Gly10−Lys18). For residues in helices II−VI, the most

pronounced perturbations in ^{1}H and ^{15}N resonances were observed for Glu52 and His89. Interestingly, substantial differences in chemical shift changes for myr(+)MA and myr(−)MA as a function of pH were observed for residues localized in the N-terminal loop and helix I. Of particular note, for myr(+)MA the $^{1}H-^{15}N$ resonance of Leu8 shifted dramatically when the pH increased from 5.5 to 8.0, while chemical shift changes of Leu8(NH) for myr(−)MA were negligible (Figure 2). Furthermore, while an increase in the solution pH for myr(+)MA and myr(−)MA led to dramatic chemical shift changes in the $^{1}H-^{15}N$ resonances of Glu52 and His89, the $^{1}H-^{15}N$ resonance of Ser9 exhibited a substantial shift only in the case of myr(−)MA. Lowering the pH of MA samples from 8.0 to 5.5 restored the original spectrum, indicating a reversible process.

The direction and, to a lesser extent, the magnitude of the chemical shift perturbations observed for myr(+)MA with an increase in pH are very similar to those observed previously upon stabilization of the myr(s) form (*20*). Previous studies have shown that the $^{1}H-^{15}N$ resonance of Leu8 is an excellent "NMR reporter" that is very sensitive to the movement of the myr group (*20*, *28*, *32*). Structural studies of myr(+)MA revealed that movement of helix I induces a conformational change by which Leu8 is repositioned to accommodate the myr group in the hydrophobic cavity (*20*, *28*). Taken together, our NMR data suggest that varying the pH caused local conformational changes in the N-terminal domain of MA, which may affect the myr(s)−myr(e) equilibrium.

Determination of the Microscopic Ionization Constant of His89. The intrinsic pK_a of the histidine imidazole group typically lies between 6.0 and 7.0 (*29*, *30*) but can vary depending on the degree of burial or exposure within proteins (*30*). For this reason and because our NMR titration data described above suggest that His89 is present in the protonated and deprotonated states at pH 5.5 and 8, respectively, we employed 2D NMR methods to precisely determine the microscopic ionization constant of the imidazole group of His89. Chemical shift perturbations of imidazole's Hε1 and Cε1 signals were monitored in the HMQC spectra as a function of pH of the NMR sample. The pK_a value of the His89 imidazole group was found to be 6.5 ± 0.1 for both myr(−)MA and myr(+)MA (Figure S2 of the Supporting Information). His89 is ~80−90% protonated at pH 5.5 and ~90% deprotonated at pH 8.0. These results are in good agreement with the data given above, which altogether suggest that altering the electronic state of the His89 side chain triggers conformational changes that affect the myr(s)−myr(e) equilibrium.

NMR Spectral Properties as a Function of pH. Structural studies of the HIV-1 myr(+)MA protein revealed that the myr switch mechanism is sensitive to protein concentration (*20*). These and all subsequent studies were conducted at pH 5.5 (*20*, *28*, *32*, *46*). 2D $^{1}H-^{15}N$ HSQC spectra obtained for myr(+)MA at concentrations of $< 100\ \mu M$ revealed that resonances of Ala3−Lys18, Arg39, and Gly49 deviate significantly from those of myr(−)MA but progressively shift toward the frequencies of myr(−)MA as the concentration is increased. However, at concentrations of $> 200\ \mu M$, the NMR signals became broad and the protein started to precipitate. Structural data indicate that increasing the protein concentration promoted myr exposure (*20*). To examine whether increasing the solution pH of myr(+)MA alters the sensitivity of the myr(s)−myr(e) equilibrium to concentration, we collected 2D HSQC NMR data at pH 7 as a function of increasing protein concentration [50, 150, and 500 μM (Figure S3 of the Supporting Information)]. Interestingly, the chemical shift changes observed for residues Ala3−Lys18 are very minimal compared to those observed previously (*20*) at pH 5.5, indicating that exposure of the myr group becomes less sensitive to the change in protein concentration at pH 7.

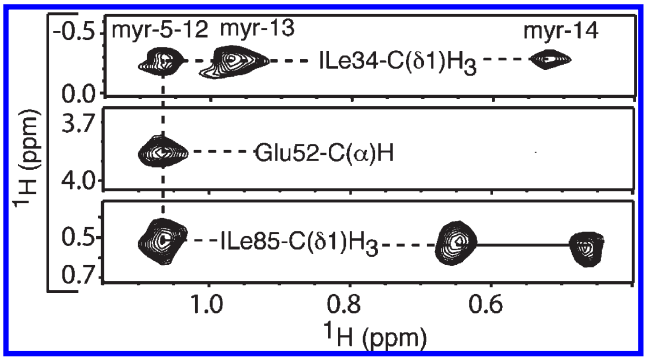

FIGURE 3: 3D ^{13}C-edited/^{12}C-double-half-filtered NOE data obtained for HIV-1 myr(+)MA at pH 7.2 showing unambiguously assigned NOE cross-peaks between the myr group and key residues of a ^{13}C-labeled protein sample (myr group unlabeled). Solid lines denote $^{1}H-^{12}C$ breakthrough doublet NOE peaks.

Because increasing the protein concentration of myr(+)MA to 500 μM did not cause significant signal broadening and/or protein precipitation, we collected a set of 2D NOESY, 3D ^{13}C-edited, and ^{15}N-edited NOE data for myr(+)MA at pH 7.2 to precisely elucidate the structural and conformational changes that may occur with a change in pH. Unambiguous NOE cross-peaks were observed between the myr group and the side chains of Val7, Leu8, Leu16, Ile34, Ala38, Glu48, Leu51, Glu52, and Ile85, indicating that the myr group is sequestered. 3D ^{13}C-edited/^{12}C-double-half-filtered NOE data collected for ^{13}C-labeled myr(+)MA with an unlabeled myr group confirmed all NOE cross-peaks between protein residues and the myr group (Figure 3). Strong NOE cross-peaks were observed between the terminal methyl group (myr-$C^{14}H_3$, ~0.5 ppm) and the side chains of Ile85 and Ile34, indicating a close packing of the myr group against these hydrophobic residues. Collectively, NMR data indicate that the myr group is buried within the core of the protein and makes contacts with the side chains of Val7, Leu8, Trp16, Ile34, Ala38, Leu51, Glu52, and Leu85. For the sake of comparison, the 3D ^{13}C-edited/^{12}C-double-half-filtered NOE data collected for ^{13}C-labeled myr(+)MA at pH 5.5 (Figure S4 of the Supporting Information) revealed that the NOE cross-peaks between the myr group and the side chains of these hydrophobic residues are weaker than the corresponding NOEs observed at pH 7.2, consistent with the finding that a significant population of myr(e) is present at pH 5.5 (*20*). Taken together, our data indicate that the structures of myr(+)MA must be similar at pH 5.5 and 7.0 and that increasing the pH does not induce major changes in the structure of the MA protein but rather stabilizes the myr(s) form.

MA Oligomerization Is Regulated by pH. SE data obtained previously for myr(+)MA at pH 5.5 best fit a monomer−trimer equilibrium with an association constant (K_a) of $2.5 \times 10^{8}\ M^{-2}$ (*20*, *32*, *46*). To study the effect of pH on the oligomerization properties of MA, we have conducted SV and SE experiments on both myr(+)MA and myr(−)MA at pH 5.5, 7.0, and 8.0. The SV profile of myr(+)MA at pH 5.5 exhibits two sedimentation boundaries. Analysis of the data using SEDFIT (*38*, *39*) yielded two peaks of approximately 1.5 S (~70%) and 2.4 S (~30%) (Figure 4). Further analysis of the SV data using molecular mass distribution revealed approximate molecular

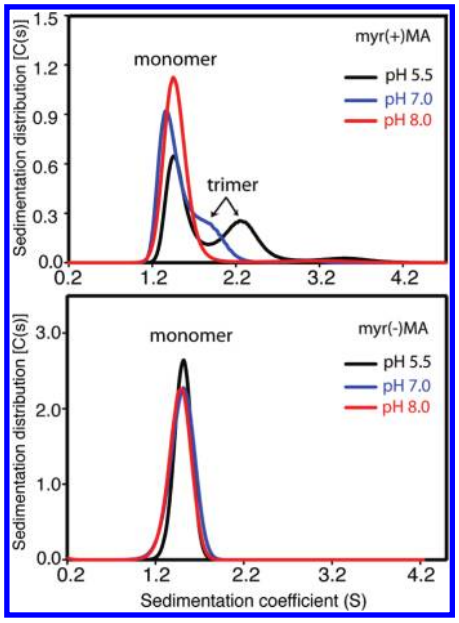

FIGURE 4: Sedimentation coefficient distributions, $c(s)$, obtained from the sedimentation profiles for myr(+)MA and myr(−)MA as a function of pH.

Table 1: Association Constants Calculated for HIV-1 MA, CA, and MACA Proteins at Different pH Values

protein	pH	equilibrium	K_a
myr(+)MA[a]	5.5	monomer−-trimer	$(1.8 \pm 0.5) \times 10^8$ M^{-2}
	7.0	monomer−trimer	$(0.7 \pm 0.1) \times 10^8$ M^{-2}
	8.0	monomer	−
myr(−)MA	5.5, 7, 8	monomer	−
myr(+)MACA	5.5	monomer−trimer	$(1.4 \pm 0.3) \times 10^{10}$ M^{-2}
	7.0	monomer−trimer	$(0.3 \pm 0.3) \times 10^{10}$ M^{-2}
	8.0	monomer−dimer	$(3.3 \pm 0.5) \times 10^4$ M^{-1}
myr(−)MACA	5.5	monomer−dimer	$(3.3 \pm 0.4) \times 10^4$ M^{-1}
	7.0	monomer−dimer	$(1.1 \pm 0.4) \times 10^5$ M^{-1}
	8.0	monomer−dimer	$(2.4 \pm 0.2) \times 10^5$ M^{-1}
myr(+)MACA (W184A/M185A)	5.5	monomer−dimer	$(6.0 \pm 0.1) \times 10^3$ M^{-1}
	7.0	monomer−dimer	$(2.0 \pm 0.3) \times 10^3$ M^{-1}
	8.0	monomer	−
CA[b]	7.0	monomer−dimer	5.5×10^4 M^{-1}

[a]This K_a is similar to that obtained in previous studies (*20*). [b]From refs *53* and *54*.

masses of 17 kDa (monomer) and 54 kDa (trimer), respectively. At pH 7, the trimer peak shifts toward the monomer peak, indicating a transient state caused by rapid dissociation of the trimer form. At pH 8, the myr(+)MA protein is present as a monomer (1.47 S). Rapid dissociation of the trimer form of myr(+)MA with an increase in pH was confirmed by SE data (Table 1 and Figure S5 of the Supporting Information). Analysis of the SE data afforded K_a values of (1.8 ± 0.5) and $(0.7 \pm 0.1) \times 10^8$ M^{-2} at pH 5.5 and 7.0 (20 °C), respectively. At pH 8.0, the SE data best fit a monomer model. On the other hand, the myr(−)MA protein exhibits a single boundary, which fits a monomer (1.5 S) at all pH values (Figure 4). Taken together, SV and SE data demonstrate that the oligomerization properties of MA are governed by pH.

HIV-1 MACA Switches from Trimer to Dimer. Because our data show that the oligomerization properties of MA can be manipulated by varying the pH, we have extended our studies to include longer constructs containing the CA domain. Extensive

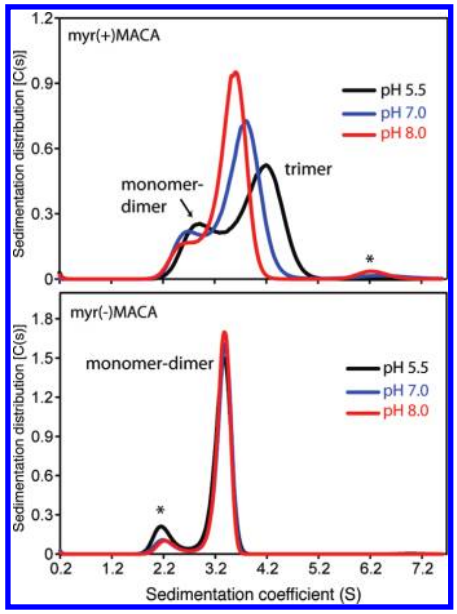

FIGURE 5: Sedimentation coefficient distributions, $c(s)$, obtained from the sedimentation profiles for myr(+)MACA and myr(−)MACA at different pH values. The small peaks marked with asterisks indicate uncharacterized minor species likely to be impurities.

analysis of Gag multimerization properties established that the CA domain plays a central role in mediating Gag−Gag interactions (*5*, *47*−*52*). In solution, the CA protein dimerizes with a dissociation constant (K_d) of 18 μM ($K_a = 5.5 \times 10^4$ M^{-1}), and dimerization is dependent on the C-terminal domain (CTD) (*53*, *54*). It has been shown that appending the CA domain to myr(+)MA increases the trimer population by ~20-fold (*20*). To assess if varying the solution pH can alter the multimerization properties of MACA, we collected SV data for myr(+)MACA proteins at pH 5.5, 7.0, and 8.0. The SV profile of myr(+)MACA at pH 5.5 exhibits two sedimentation boundaries. As shown in Figure 5, analysis of the data yielded two peaks of approximately 3.0 S (30%) and 4.3 S (~70%). At pH 7, the major peak shifts toward a lower S value (3.7 S), consistent with a lower-molecular mass species, while the minor peak shifted slightly to a lower sedimentation coefficient value (2.75 S). Increasing the pH to 8 led to shifting of the major and minor peaks to 3.6 and 2.7 S, respectively (Figure 5). Notice that the two peaks overlap at the higher pH, indicating a rapid dissociation of the major species.

As mentioned above, previous SE data at pH 5.5 revealed that myr(+)MACA is in a monomer−trimer equilibrium (*20*), so it is reasonable to suggest that the two peaks at 4.3 and 3.0 S represent the trimer and monomer species, respectively. However, because the sedimentation coefficients of both the major and minor peaks are sensitive to pH, we hypothesized that the minor peak probably represents a fast monomer−dimer equilibrium. To test this hypothesis, we have collected SE data for myr(+)MACA as a function of pH (Figure S6 of the Supporting Information). At pH 5.5, SE data best fit a monomer−trimer equilibrium with a K_a of $(1.4 \pm 0.3) \times 10^{10}$ M^{-2}. The K_a is decreased by 4-fold when the pH is increased from 5.5 to 7.0 (Table 1), indicating rapid dissociation of the trimer form. Interestingly, the SE data for myr(+)MACA at pH 8 best fit a monomer−dimer equilibrium and afforded a K_a of $(3.3 \pm 0.5) \times 10^4$ M^{-1}, which is similar to that observed for the CA domain (*53*, *54*).

One explanation for the pH dependency of the s value of the minor species in the SV data is that myr(+)MACA resides in a

monomer−dimer−trimer equilibrium, but the dimeric intermediate is not significantly populated. To test this possibility, we subjected the sedimentation equilibrium data to nonlinear square fitting analysis using a monomer−dimer−trimer model. The dimerization equilibrium constant tends to yield a very small value (near zero), consistent with the hypothesis that there is little information in the data for a third species. In summary, the data are best described by a monomer−trimer equilibrium. However, we cannot rule out the possibility of a dimeric state that is not significantly populated under these conditions.

This alternative model has been tested by various approaches. First, we examined whether dimerization of CA is pH-dependent. To do so, we collected SV data for myr(−)MACA and CA as a function of pH. The SV profile of myr(−)MACA exhibits one major sedimentation boundary that is insensitive to pH. As shown in Figure 5, analysis of the data yielded two peaks of approximately 3.4 S (∼95%) and 2.2 S (< 5%). The SE data (not shown) confirmed that the major boundary represents a monomer−dimer equilibrium with K_a varying slightly as a function of pH (Table 1). The second minor peak at 2.2 S is likely an impurity because it was not observed in other samples. Likewise, SV data obtained for CA at pH 5.5, 7.0, and 8.0 show a single boundary (∼2.7 S) at all pH values (Figure S7 of the Supporting Information), indicating an intermediate value representing a monomer−dimer equilibrium (*53*, *54*).

The second approach involved alteration of the monomer−dimer properties of MACA by mutagenesis. We generated a myr(+)MACA double mutant with Trp184 and Met185 in the CA domain substituted with alanine residues (W184A/M185A). These amino acid substitutions were shown to significantly inhibit CA dimerization (*53*). Interestingly, SV data obtained for myr(+)MACA-W184A/M185A at pH 5.5 yielded a single boundary with a sedimentation coefficient value of 2.7 S (Figure S8 of the Supporting Information), which indicates that the formation and stability of the trimer form of MACA are dependent on the dimer interface of CA. The finding that myr(+)MACA trimerization is disrupted by mutation of Trp184 and Met185 is very similar to that observed for myr(−)GagΔp6 bound to inositol phosphates (*55*). Increasing the pH shifted the *s* values only slightly to 2.55 and 2.5 S at pH 7 and 8, respectively. Because SV and SE data of CA and myr(−)MACA revealed that dimerization of CA is not pH-dependent, the sensitivity of the sedimentation coefficient to pH in myr(+)MACA-W184A/M185A is likely to be attributed to the MA domain. The nature of the oligomerization for myr(+)MACA-W184A/M185A was determined by SE data. At pH 5.5, SE data analysis best fit a monomer−dimer equilibrium with a K_a of $(6.0 \pm 0.1) \times 10^3$ M^{-1} (Figure S9 of the Supporting Information). Because the sedimentation coefficient and sensitivity to pH of the minor peak for WT myr(+)MACA (Figure 5) are very similar to that observed for myr(+)MACA-W184A/M185A, it is very likely that the minor peak at 3.0 S (Figure 5) represents monomer and dimer species that are in fast exchange. Taken together, our data demonstrate that the myr(s)−myr(e) equilibrium in a Gag-like construct is also sensitive to pH and that the MA domain can dictate the type of multimers in solution at any given pH.

NMR and Biophysical Characterization of MA Mutants That Disrupt the His−Glu Salt Bridge. Previous studies have shown that mutations in helix V of the MA domain, including L85R, Y86G, C87S, V88E, and H89G, led to retargeting of the majority of virus particle formation to intracellular compartments and severely defective virus replication in the CEM(12D-7) cell line (*18*). Structural characterization of the myr(+)MA protein (*20*) revealed that these residues are located in or near the hydrophobic cavity occupied by the myr group and may contribute to the stabilization of the pocket. Thus, it is likely that disrupting the hydrophobic cavity and altering the myr switch mechanism contribute to the retargeting of Gag to intracellular compartments.

To confirm that importance of the salt bridge in regulating the myr(s)−myr(e) equilibrium, we made H89G and E12A MA mutants and examined their structural properties by NMR and biophysical methods. Protein expression and purification were achieved according to a standard protocol (*20*, *28*, *32*). However, in sharp contrast to the WT myr(+)MA protein, the myr(+)MA-H89G protein was found exclusively in inclusion bodies and was extracted under denaturing conditions. The protein was poorly soluble (concentration of ∼40 μM). NMR and SV data for myr(+)MA-H89G (Figures S10 and S11 of the Supporting Information) revealed that the protein forms high-molecular mass aggregates that caused considerable broadening in the NMR signal. SV data show multiple peaks with large sedimentation coefficient values. Changes in the pH do not appear to affect the type or nature of myr(+)MA-H89G aggregates.

To assess whether the His89 mutation caused unfolding in the tertiary structure of MA and/or induced dramatic conformational changes leading to the formation of high-molecular mass aggregates, the myr(-)MA-H89G mutant was made and characterized by the same methods. Interestingly, the protein was soluble and present in the monomeric state (Figure S11 of the Supporting Information). CD data confirmed that the MA protein maintains its secondary structure in the context of the H89G mutation (Figure S12 of the Supporting Information). These results suggest that substitution of His89 not only disrupted the His−Glu salt bridge but also destabilized the tertiary structure, triggering myr exposure and promoting high-order protein self-association.

Because the imidazole group of His89 is also engaged in another intramolecular H-bond with the carbonyl group of Leu51, substitution with a Gly may cause larger conformational changes that may contribute to the loss of stability of the hydrophobic pocket and in turn to disruption of the myr switch mechanism. We predicted that substitution of Glu12 is less complex. To examine this possibility, we have substituted Glu12 with Ala and examined its biophysical characteristics by NMR and sedimentation methods. Both myr(−)MA-E12A and myr(+)MA-E12A proteins were made. Both proteins were very soluble, and purification was achieved as described for WT proteins. These substitutions did not adversely affect myristylation efficiencies [∼100%, compared to ∼90% myr and 10% myr(−) for the wild-type MA protein]. ^{1}H and ^{15}N NMR signals observed in two-dimensional (2D) ^{1}H−^{15}N HSQC spectra of myr(+)MA and myr(−)MA were substantially different for the first ∼20 amino acids, indicating sequestration of the myr group (Figure S13 of the Supporting Information). Indeed, SV data confirmed that the myr(+)MA-E12A protein is a monomer and insensitive to changes in pH (Figure S13 of the Supporting Information). Collectively, our data demonstrate that disruption of the His89−Glu12 salt bridge alters the myr(s)−myr(e) equilibrium, although substitution of His89 appears to have a much larger effect on the stability of the hydrophobic cavity.

As discussed earlier, substitution of Trp184 and Met185 with Ala residues in myr(+)MACA inhibited the formation of the trimer form. However, SV and SE data revealed that myr(+)MACA-W184A/M185A resides in a monomer−dimer equilibrium where

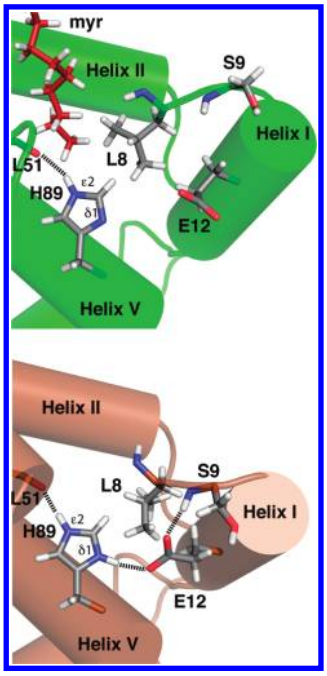

FIGURE 6: Structural view of the HIV-1 myr(+)MA protein in the myr-sequestered (green) and myr-exposed (brown) forms. Notice the conformational change involving Leu8, which acts as an NMR reporter for the movement of the myr group.

dimerization appears to be induced by the MA domain. Because substitution of Glu12 with Ala completely abolished trimer formation for myr(+)MA, we predicted that the E12A mutation in MACA will modulate the oligomerization properties of MACA. As shown in Figure S14 of the Supporting Information, the SV profile of myr(+)MACA-E12A/W184A/M185A exhibits a single sedimentation boundary that is insensitive to pH. Analysis of the data yielded one peak at 2.4 S, consistent with the monomeric character of myr(+)MACA. In summary, we conclude that substitution of Glu12 modulates the myr(s)−myr(e) equilibrium of MA and MACA in vitro.

His−Glu Salt Bridge, an Important Structural Element in HIV-1 MA. It has been established that for a stable salt bridge to form between oppositely charged residues (such as Asp or Glu with Arg, Lys, or His), the two following criteria become critical (*56*, *57*). (i) The centroids of the side chain charged groups in oppositely charged residues are within 4 Å of each other (*58*), and (ii) at least one pair of Asp or Glu side chain COO- oxygen atoms and side chain nitrogen atoms of Arg, Lys, or His are within 4.0 Å of each other. To verify the formation of a salt bridge between the side chains of His89 and Glu12 in HIV-1 myr(−)MA, distances between the centroid of COO- and the His89 nitrogen atom were measured and found to be within 4 Å in both X-ray and NMR structures of myr(−)MA (Figure S15 of the Supporting Information) (*20*, *28*, *59*). However, this distance is significantly larger in the myr(+)MA structure (*20*, *28*).

As described above, significant structural differences between the myr(e)MA and myr(s)MA proteins involve the positioning and packing of helix I (*20*, *21*, *28*). For both myr(e)MA and myr(s)MA, the imidazole group of His89 is locked in a unique orientation in which Nε2 forms a salt bridge with the carbonyl group of Leu51. For myr(e)MA, tight packing of helix I against helices II and V is stabilized by a Glu12(COO-)−His89(Hδ2) salt bridge and Glu12(COO-)−Ser9(NH) hydrogen bond (Figure 6). As shown in Figure 2, increasing the solution pH for myr(−)MA

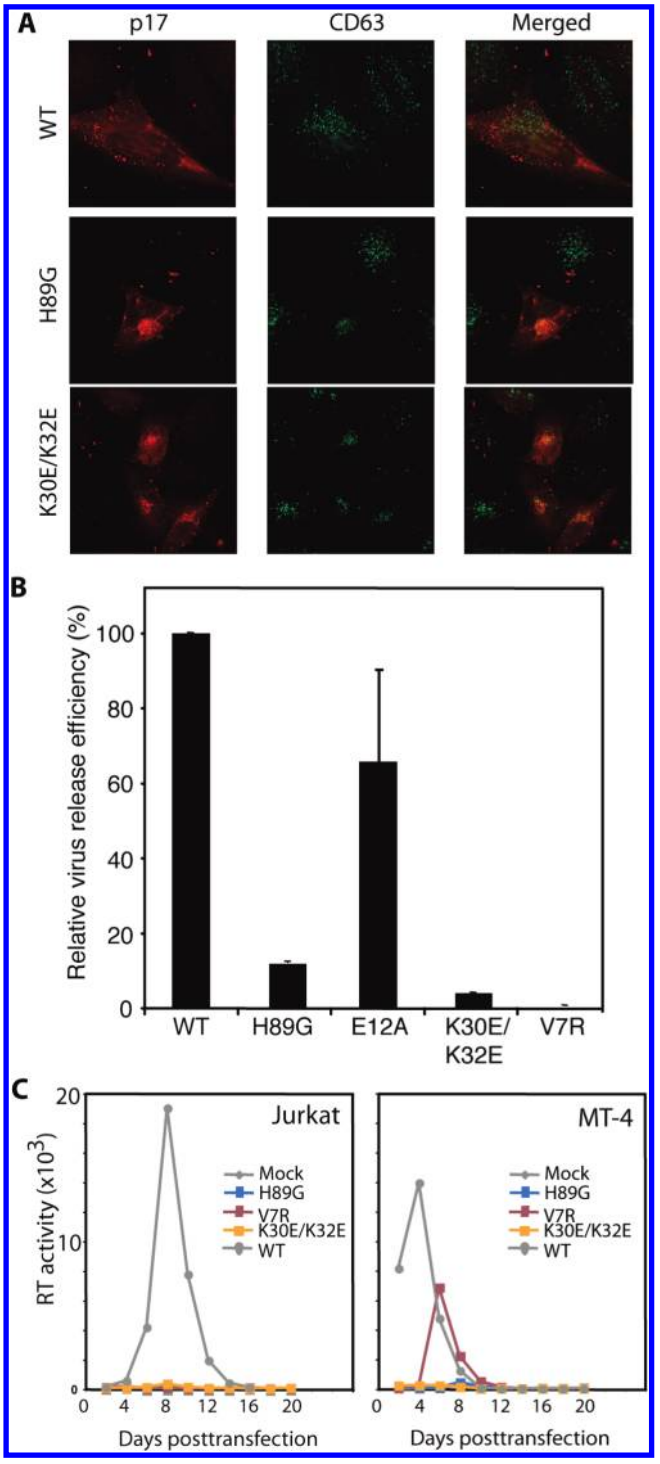

FIGURE 7: (A) Subcellular localization of WT HIV-1 Gag compared to that of the H89G and K30E/K32E mutants. HeLa cells were transfected with the indicated molecular clones. Cells were fixed and stained with an antibody specific for p17 (MA) or were costained with antibodies specific for p17 (MA) and the MVB marker CD63. (B) Virus release efficiency data for WT and mutant Gag [calculated as follows: virus release efficiency = virion p24/(cell Gag + virion Gag)]. (C) The MA H89G mutant induces defects in virus replication in T-cells. Jurkat or MT-4 T-cells were transfected with WT pNL4-3 or the indicated MA mutant derivatives. Cells were split every 2 days; virus replication was measured by RT assay. For comparison, virus replication data for V7R and K30E/K32E mutants are also shown.

led to dramatic chemical shift changes of the HN resonances of Ser9, Glu52, and His89. These residues are directly involved in a web of hydrogen bonds that stabilize the packing of helix I. In comparison, helix I is moved away in myr(s)MA to allow for

sequestration of the myr group, and contacts between Glu12-(COO-) and both His89(Hδ2) and Ser9(NH) are no longer present (Figure 6). Our data clearly show that manipulation of the electronic properties of the imidazole group of His89 via variation of the solution pH drastically alters the myr(s)−myr(e) equilibrium.

The Subcellular Site of HIV-1 Gag Assembly Is Altered by the H89G Mutation. A previous study demonstrated that the subcellular site of HIV-1 Gag assembly is altered by the H89G mutation (*18*). However, the identity of the site at which the H89G mutant assembles has not been previously defined. To address this issue, we performed dual immunostaining with an anti-MA antibody and an antibody specific for the tetraspanin CD63 in HeLa cells transfected with WT and the H89G mutant molecular clones. CD63 is commonly used as a marker for the late endosomal/MVB compartment (*60*, *61*). The H89G mutant displayed an internal localization distinct from the largely PM distribution observed with the WT. The internal Gag puncta observed with H89G colocalized extensively with CD63, suggesting MVB localization (Figure 7A). As a control, we also included the K30E/K32E mutant, previously shown to be MVB-targeted (*43*). These results indicate that the H89G and L30E/K32E mutants are targeted to the same internal, CD63-positive compartment. Consistent with previous results (*18*), we also determined by radio-immunoprecipitation analysis that the H89G mutant displayed a marked reduction in the efficiency of virus particle production, as did the V7R mutant, previously shown to be defective for Gag−membrane association (*45*) due to a defect in myristate exposure (*32*) (Figure 7B). Although the V7R mutation reduces the amount of cell-associated p24, the overall Gag expression level for this mutant is similar to that of WT Gag (Figure S16 of the Supporting Information). Gag expression and processing profiles for the H89G were similar to those of the WT (Figure S16 of the Supporting Information). Taken together, these results indicate that His89 is essential for proper targeting of Gag to the PM and efficient particle formation in HeLa cells.

As discussed above, previous studies have shown that the H89G mutation led to severely defective virus replication in the CEM(12D-7) T-cell line (*18*). To verify whether this phenotype is cell type-dependent, we assessed the effect of the H89G mutation on virus replication in additional T-cell lines. The Jurkat and MT-4 T-cell lines were transfected with molecular clones encoding WT or H89G mutant MA. As controls, we included the previously described V7R and K30E/K32E mutants (*43*, *45*). The results demonstrated that the H89G mutation blocked virus replication in both T-cell lines (Figure 7C). In comparison, the V7R mutant replicated with a delay of ~6 days in MT-4 cells but did not replicate in Jurkat cells (Figure 7C). These results indicate that the H89G mutant is replication defective in a range of T-cell lines.

Our NMR and biophysical studies revealed that the E12A mutation led to tight sequestration of the myr group and inhibited trimer formation. To test whether this mutation has an effect on virus production, HeLa cells transfected with WT or E12A mutant molecular clones were metabolically radiolabeled, and cell and virus lysates were immunoprecipitated with HIV-Ig. Our data show that E12A had only a small effect on virus production compared to H89G (Figure S16 of the Supporting Information), suggesting that salt bridge partners have very different effects on virus production. In addition, we performed dual immunostaining with an anti-MA antibody and an antibody specific for the tetraspanin CD63 in HeLa cells transfected with the E12A mutant molecular clone. The E12A mutant exhibited a localization pattern similar to that of WT Gag (Figure S16 of the Supporting Information).

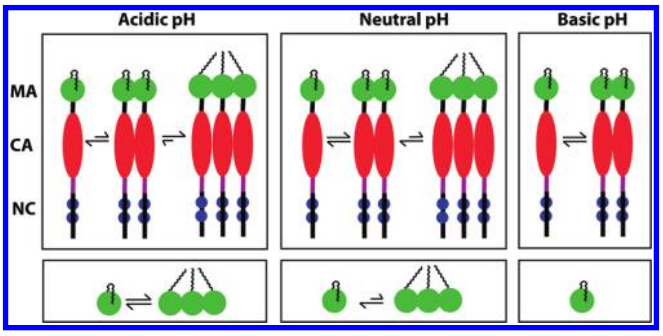

FIGURE 8: Schematic representation showing multimerization events of Gag and MA proteins as a function of pH.

DISCUSSION

Structural studies have demonstrated that the myr group of HIV-1 MA can adopt sequestered and exposed conformations (*20*). Exposure of the myr group is coupled with protein trimerization and is enhanced by factors that promote protein self-association, such as increasing protein concentration or appending the CA domain (*20*). Here we provide evidence that myr exposure in HIV-1 MA is modulated by pH. We also show that extrusion of the myr group becomes less sensitive to protein concentration and attachment of CA at pH ≥7. Intriguingly, increasing the pH to 8 inhibited the formation of trimers for MA and MACA (Figure 8). These findings indicate that trimerization of Gag in vitro, although enhanced by CA, is solely driven by the MA domain and tightly regulated by pH.

HIV-1 Gag myristoylation and multimerization are directly linked to efficient membrane binding and are required for particle formation and viral infectivity (*13*, *44*, *62*, *63*). The oligomerization properties of HIV-1 Gag, MA, and MACA constructs have been extensively studied (*13*, *20*, *32*, *46*, *49*, *55*, *64*−*68*). The CA domain is known to play a central role in mediating Gag−Gag interactions (*5*, *47*−*52*). Other domains, including SP1 and NC, are also thought to play important roles in Gag assembly (*2*, *47*, *52*, *63*, *65*, *69*−*71*). Despite the evidence that MA can form trimers and assemble on the membrane as hexamers (*68*, *72*), the role of MA−MA interactions in stabilizing Gag−Gag interactions is still controversial (*20*, *55*, *64*−*66*, *68*, *73*). While it appears that interactions between the myr group and membrane are essential for Gag−Gag interactions in living cells (*13*), electron cryotomography studies of immature virions revealed that CA and SP1 form ordered hexagonal shells, but MA and NC shells lack an ordered structure (*52*). Our findings support the hypothesis that myristoylation is important for Gag multimerization and reveal that pH is an additional factor that governs the type of Gag multimers in solution.

Rein and co-workers have recently examined the oligomerization properties of Gag in the absence or presence of inositol phosphates (*55*). The Gag construct used in these studies lacks the myr group and the p6 domain [myr(−)GagΔp6]. SE data obtained for myr(−)GagΔp6 at pH 7.4 indicate that the protein is in a monomer−dimer equilibrium with a K_d of 5.5 μM (K_a = 1.8×10^5 M^{-1}) or 14 μM (K_a = 6.7×10^4 M^{-1}) depending on the method of measurement. Interestingly, these K_d values are very similar to that obtained for myr(−)MACA at a similar pH value

(Table 1), suggesting that the NC domain has minimal or no role in Gag multimerization in the absence of bound RNA. At this point, it is not clear whether inositol phosphate-driven multimerization of MA and Gag proteins is pH-dependent.

Implications for Gag−Membrane Binding. It is now established that PI(4,5)P_2 is critical for HIV-1 and HIV-2 Gag assembly and binding to the PM (*21*−*23*, *28*). Recent studies have revealed that targeting of Moloney murine leukemia virus (MMLV) Gag to the PM is also PI(4,5)P_2-dependent (*74*). Earlier studies revealed that HIV-1 and MMLV are enriched in phosphoinositides, including PI(4,5)P_2 (*75*). Consistent with these findings, in vitro studies have shown that binding of HIV-1 Gag (*23*), MA and MACA (*76*), and MMLV MA (*74*) to membrane models is enhanced by addition of PI(4,5)P_2 and phosphatidylserine (*76*). Despite our current understanding of the effect of pH on the myr(s)−myr(e) equilibrium and the possible consequences for membrane binding, it has yet to be established whether actual binding of MA and Gag to membranes in vivo is pH-dependent. In vitro studies of Gag assembly have provided insights into the process of Gag−Gag interactions and multimerization. Gag is capable of forming VLPs in vitro in the absence of other viral and cellular constituents (*1*, *2*). Authentic-like particles can be formed by addition of RNA or inositol phosphates to Gag (*1*, *2*, *77*). Various biochemical assays have been devised for the study of binding of MA, MACA, and Gag proteins to membrane models. In these experiments, liposomes were at pH 7−8 and often yielded variable binding affinities (*17*, *67*, *76*, *78*). On the basis of our findings, it is reasonable to suggest that changes in pH may have an effect on the affinity of MA and Gag binding to membranes.

Relationship between the His−Glu Salt Bridge and Virus Production. A significant point that emerged from this study is the interplay among Gag targeting, membrane binding, and virus production. Here we show that mutation of His89 induced the retargeting of the Gag protein to MVBs and severely reduced virus replication. Interestingly, the in vivo phenotype exhibited by the Gag H89G mutant is very different from that of G2A, V7R, or L8I and L8A mutants, which displayed a hazy, nonpunctate staining pattern typical of HIV-1 Gag mutants that are defective in membrane binding (*18*, *32*, *45*, *79*, *80*). Structural studies revealed that Val7 and Leu8 mutations shut off the myr switch and stabilize the myr(s) form (*32*). Thus, it appears that sequestration or the lack of a myr group favors cytosolic localization rather than MVB association. Despite the extensive analysis of the effect of Gag mutations on intracellular localization and their effect on virus production and infectivity, it is not yet clear how and why some Gag mutants are associated with MVBs. Although earlier studies have shown that targeting of the Gag K30E/K32E mutant to MVB compartments led to severely defective virus particle production in HeLa cells (*43*), recent evidence revealed that it can still support highly efficient assembly and release in T-cells (*10*). It was suggested that under some circumstances, late endosomal compartments can serve as productive sites for HIV assembly in some cell types (*10*).

On the basis of the current understanding of the effect of some MA mutations on the myr switch mechanism, it is reasonable to suggest that formation of Gag aggregates caused by substitution of His89 (and possibly other residues in the vicinity) may be responsible for association with MVBs. Structural, biophysical, and biochemical characterizations of MA mutants may help in explaining localization pathways of Gag.

Our structural and biophysical data for the E12A mutant clearly indicate that the myr group is tightly sequestered. One possibile explanation for this finding is that mutation of E12 could disrupt the E12−S9 salt bridge and favor the myr(s) form. However, because our data demonstrate that myr exposure is modulated by pH and that deprotonation of His89 appears to be important in the regulation of the myr switch mechanism in vitro, the E12−S9 salt bridge must be of a secondary importance or inconsequential. The slight effect of the E12A mutation on virus production and WT-like Gag subcellular localization suggests either that the His−Glu salt bridge is not very important for replication or that other factors contributing to Gag targeting and assembly may still be involved. For example, it has yet to be determined whether binding of PI(4,5)P_2 to MA-E12A triggers myr exposure and promotes oligomerization. Efficient virus production is directly linked to Gag−PI(4,5)P_2 binding and subsequent myr exposure. We have shown that the myr group in HIV-2 MA is tightly sequestered and that PI(4,5)P_2 binding, although identical to that of HIV-1, is unable to trigger exposure of the myr group (*21*). However, our in vivo data revealed that the efficiency of HIV-2 virus production is very similar to that of HIV-1 (*27*). In other words, we believe the interplay among myr exposure, Gag targeting, and virus production is more complex than we initially thought.

Implications for Other Retroviral Gag Proteins. Several structures of retroviral myr(−)MA(*81*−*86*) and myr(+)MA proteins (*20*, *21*) have been determined by NMR or X-ray methods. In contrast to their low degree of sequence homology, structures of retroviral MA proteins are remarkably similar. Phylogenetic sequence analysis revealed that His89 is highly conserved across all known strains of HIV-1, HIV-2, and SIV, suggesting that its structural role in regulating the myr switch mechanism is probably important for Gag assembly, virus infectivity, and production at least in the lentivirus genus. Despite their high degree of homology of sequence and structure, the myr switch mechanism is significantly different for HIV-1 and HIV-2 MA proteins (*21*). The myr group of HIV-2 MA is tightly sequestered, and the protein is a monomer (*21*). These observations indicate that key differences in the myr switch mechanism can exist between closely related retroviruses. In HIV-2 MA, Glu12 is substituted with Lys. Previous studies have shown that the pK_a value of a buried Lys residue can be abnormally low (~5.6) compared to those of Lys residues that are usually found at the surface and interact extensively with water (pK_a ~ 10.5) (*87*). In this case, a Lys side chain is present in the neutral state (NH_2). The pK_a values of the side chains of His89 and Lys12 in HIV-2 MA are not known, and thus, it is unclear whether a varying pH can trigger myr exposure in HIV-2 MA.

In summary, we have now established that the MA domain of HIV-1 Gag acts as a "pH sensor" and that, at least in vitro, myr exposure is regulated by pH. We also suggest that our results may have broader implications for the nature and type of Gag multimers present in vivo. A potential role of pH variations in subcellular localization and targeting of the HIV-1 Gag protein is not known. Fluctuations in intracellular pH (from 6.3 to 7.8) are often observed in response to cell growth, development, and apoptosis (*88*−*90*). Even alterations in PM function can be induced by cytopathic viruses, including HIV-1 (*91*). A significant decrease in pH from 7.2 to as low as 6.0 was observed in cells infected by HIV-1 (*91*). As suggested by one reviewer of this work, our findings may suggest that given that the intracellular pH in healthy cells is around 7−7.2, Gag multimerization-induced

myristate exposure would occur only under specific conditions (e.g., with cytopathic effects). Thus, exposure of the myr group upon Gag multimerization is probably not triggered unconditionally. While it has yet to be established whether manipulation of intracellular pH can alter kinetic pathways and sites or efficiency of Gag assembly, this possibility warrants further investigation.

ACKNOWLEDGMENT

We thank Dr. Michael F. Summers (Howard Hughes Medical Institute, University of Maryland, Baltimore County) for providing the MA co-expression molecular clone.

SUPPORTING INFORMATION AVAILABLE

2D $^{1}H-^{15}N$ HSQC NMR spectra of myr(−)MA and myr(+)MA as a function of pH (Figures S1 and S2); 3D ^{13}C-edited/^{12}C-double-half-filtered NOE spectrum of myr(+)MA at pH 5.5 (Figure S3); sedimentation equilibrium profiles for myr(+)MA at different pH values (Figure S4); plots of chemical shift changes versus pH used to determine the pK_a value of His89 for myr(−)MA (Figure S5); sedimentation equilibrium and velocity profiles for WT CA and various MACA mutants as a function of pH (Figure S6−S9); 2D NMR HSQC spectra (Figure S10), sedimentation velocity profiles (Figure S11), and CD spectra (Figure S12) for MA H89G mutants; 2D HSQC spectra and sedimentation velocity profiles of MA E12A mutants (Figure S13); sedimentation velocity profiles for myr(+)MA-E12A/W184A/M185A as a function of pH (Figure S14); structural representation of salt bridge formation in the HIV-1 MA structures (Figure S15); and SDS−PAGE showing the effect of His89 and E12 mutations on virus production (Figure S16). This material is available free of charge via the Internet at http://pubs.acs.org.

REFERENCES

1. Campbell, S., Fisher, R. J., Towler, E. M., Fox, S., Issaq, H. J., Wolfe, T., Phillips, L. R., and Rein, A. (2001) Modulation of HIV-like particle assembly in vitro by inositol phosphates. *Proc. Natl. Acad. Sci. U.S.A. 98*, 10875–10879.
2. Campbell, S., and Rein, A. (1999) In vitro Assembly Properties of Human Immunodeficiency Virus Type 1 Gag Protein Lacking the p6 Domain. *J. Virol. 73*, 2270–2279.
3. Chu, H., Wang, J. J., and Spearman, P. (2010) Human Immunodeficiency Virus Type-1 Gag and Host Vesicular Trafficking Pathways. *Curr. Top. Microbiol. Immunol. 339*, 67–84.
4. Adamson, C. S., and Freed, E. O. (2007) Human Immunodeficiency Virus Type 1 Assembly, Release and Maturation. *Adv. Pharmacol. 55*, 347–387.
5. Ganser-Pornillos, B. K., Yeager, M., and Sundquist, W. I. (2008) The structural biology of HIV assembly. *Curr. Opin. Struct. Biol. 18*, 203–217.
6. Ono, A. (2009) HIV-1 assembly at the plasma membrane: Gag trafficking and localization. *Future Virol. 4*, 241–257.
7. Finzi, A., Orthwein, A., Mercier, J., and Cohen, E. A. (2007) Productive Human Immunodeficiency Virus Type 1 Assembly Takes Place at the Plasma Membrane. *J. Virol. 81*, 7476–7490.
8. Gousset, K., Ablan, S. D., Coren, L. V., Ono, A., Soheilian, F., Nagashima, K., Ott, D. E., and Freed, E. O. (2008) Real-time visualization of HIV-1 GAG trafficking in infected macrophages. *PLoS Biol. 4*, e1000015.
9. Hermida-Matsumoto, L., and Resh, M. D. (2000) Localization of Human Immunodeficiency virus Type 1 Gag and env at the Plasma Membrane by Confocal Imagine. *J. Virol. 74*, 8670–8679.
10. Joshi, A., Ablan, S. D., Soheilian, F., Nagashima, K., and Freed, E. O. (2009) Evidence that productive human immunodeficiency virus type 1 assembly can occur in an intracellular compartment. *J. Virol. 83*, 53755387.
11. Jouvenet, N., Bieniasz, P. D., and Simon, S. M. (2008) Imaging the biogenesis of individual HIV-1 virions in live cells. *Nature 454*, 236–240.
12. Jouvenet, N., Neil, S. J. D., Bess, C., Johnson, M. C., Virgen, C. A., Simon, S. M., and Bieniasz, P. D. (2006) Plasma membrane is the site of productive HIV-1 particle assembly. *PLoS Biol. 4*, 2296–2310.
13. Li, H., Dou, J., Ding, L., and Spearman, P. (2007) Myristoylation is required for human immunodeficiency virus type 1 Gag-Gag multimerization in mammalian cells. *J. Virol. 81*, 12899–12910.
14. Ono, A. (2010) Relationships between plasma membrane microdomains and HIV-1 assembly. *Biol. Cell 102*, 335–350.
15. Welsch, S., Keppler, O. T., Habermann, A., Allespach, I., Krijnse-Locker, J., and Kräusslich, H.-G. (2007) HIV-1 buds predominantly at the plasma membrane of primary human macrophages. *PLoS Pathog. 3*, e36.
16. Bryant, M., and Ratner, L. (1990) Myristoylation-Dependent Replication and Assembly of Human Immunodeficiency Virus 1. *Proc. Natl. Acad. Sci. U.S.A. 87*, 523–527.
17. Spearman, P., Horton, R., Ratner, L., and Kuli-Zade, I. (1997) Membrane binding of human immunodeficiency virus type 1 matrix protein in vivo supports a conformational myristyl switch mechanism. *J. Virol. 71*, 6582–6592.
18. Freed, E. O., Orenstein, J. M., Buckler-White, A. J., and Martin, M. A. (1994) Single Amino Acid Changes in the Human Immunodeficiency Virus Type 1 Matrix Protein Block Virus Particle Production. *J. Virol. 68*, 5311–5320.
19. Ono, A., Orenstein, J. M., and Freed, E. O. (2000) Role of the Gag Matrix Domain in Targeting Human Immunodeficiency Virus Type 1 assembly. *J. Virol. 74*, 2855–2866.
20. Tang, C., Loeliger, E., Luncsford, P., Kinde, I., Beckett, D., and Summers, M. F. (2004) Entropic switch regulates myristate exposure in the HIV-1 matrix protein. *Proc. Natl. Acad. Sci. U.S.A. 101*, 517–522.
21. Saad, J. S., Ablan, S. D., Ghanam, R. H., Kim, A., Andrews, K., Nagashima, K., Soheilian, F., Freed, E. O., and Summers, M. F. (2008) Structure of the myristylated HIV-2 MA protein and the role of phosphatidylinositol-(4,5)-bisphosphate in membrane targeting. *J. Mol. Biol. 382*, 434–447.
22. Ono, A., Ablan, S. D., Lockett, S. J., Nagashima, K., and Freed, E. O. (2004) Phosphatidylinositol (4,5) bisphosphate regulates HIV-1 Gag targeting to the plasma membrane. *Proc. Natl. Acad. Sci. U.S.A. 101*, 14889–14894.
23. Chukkapalli, V., Hogue, I. B., Boyko, V., Hu, W.-S., and Ono, A. (2008) Interaction between HIV-1 Gag matrix domain and phosphatidylinositol-(4,5)-bisphosphate is essential for efficient Gag-membrane binding. *J. Virol. 82*, 2405–2417.
24. Chukkapalli, V., Oh, S. J., and Ono, A. (2010) Opposing mechanisms involving RNA and lipids regulate HIV-1 Gag membrane binding through the highly basic region of the matrix domain. *Proc. Natl. Acad. Sci. U.S.A. 107*, 1600–1605.
25. Martin, T. F. J. (2001) PI(4,5)P2 regulation of surface membrane traffic. *Curr. Opin. Cell Biol. 13*, 493–499.
26. Behnia, R., and Munro, S. (2005) Organelle identity and the signposts for membrane traffic. *Nature 438*, 597–604.
27. McLaughlin, S., and Murray, D. (2005) Plasma membrane phosphoinositide organization by protein electrostatics. *Nature 438*, 605–611.
28. Saad, J. S., Miller, J., Tai, J., Kim, A., Ghanam, R. H., and Summers, M. F. (2006) Structural basis for targeting HIV-1 Gag to virus assembly sites on the plasma membrane. *Proc. Natl. Acad. Sci. U.S.A. 103*, 11364–11369.
29. Liu, T., Ryan, M., Dahlquist, F. W., and Griffith, O. H. (1997) Determination of pK_a values of the histidine side chains of phosphatidylinositol-specific phospholipase C from *Bacillus cereus* by NMR spectroscopy and site-directed mutagenesis. *Protein Sci. 6*, 1937–1944.
30. Edgcomb, S. P., and Murphy, K. P. (2002) Variability in the pK_a of histidine side-chains correlates with burial within proteins. *Proteins: Struct., Funct., Genet. 49*, 1–6.
31. Massiah, M. A., Starich, M. R., Paschall, C., Summers, M. F., Christensen, A. M., and Sundquist, W. I. (1994) Three dimensional structure of the human immunodeficiency virus type 1 matrix protein. *J. Mol. Biol. 244*, 198–223.
32. Saad, J. S., Loeliger, E., Luncsford, P., Liriano, M., Tai, J., Kim, A., Miller, J., Joshi, A., Freed, E. O., and Summers, M. F. (2007) Point mutations in the HIV-1 matrix protein turn off the myristyl switch. *J. Mol. Biol. 366*, 574–585.
33. Lanman, J., Sexton, J., Sakalian, M., and Prevelige, P. E., Jr. (2002) Kinetic analysis of the role of intersubunit interactions in human immunodeficiency virus type 1 capsid protein assembly *in vitro*. *J. Virol. 76*, 6900–6908.
34. Delaglio, F., Grzesiek, S., Vuister, G. W., Zhu, G., Pfeifer, J., and Bax, A. (1995) NMRPipe: A multidimensional spectral processing system based on UNIX pipes. *J. Biomol. NMR 6*, 277–293.

35. Johnson, B. A., and Blevins, R. A. (1994) NMRview: A Computer Program for the Visualization and Analysis of NMR Data. *J. Biomol. NMR 4*, 603–614.
36. Folkers, P. J. M., Folmer, R. H. A., Konings, R. N. H., and Hilbers, C. W. (1993) Overcoming the ambiguity problem encountered in the analysis of nuclear Overhauser magnetic resonance spectra of symmetric dimer proteins. *J. Am. Chem. Soc. 115*, 3798–3799.
37. Wüthrich, K. (1986) NMR of Proteins and Nucleic Acids, John Wiley & Sons, New York.
38. Schuck, P. (2003) On the analysis of protein self-association by sedimentation velocity analytical ultracentrifugation. *Anal. Biochem. 320*, 104–124.
39. Schuck, P., Perugini, M. S., Gonzales, N. R., Howlett, G. J., and Schubert, D. (2002) Size-distribution analysis of proteins by analytical ultracentrifugation: Strategies and application to model systems. *Biophys. J. 82*, 1096–1111.
40. Johnson, M. L., and Faunt, L. M. (1992) Parameter estimation by least-squares methods. *Methods Enzymol. 210*, 1–37.
41. Cole, J. L. (2004) Analysis of heterogeneous interactions. *Methods Enzymol. 384*, 212–232.
42. Adachi, A., Gendelman, H. E., Koenig, S., Folks, T., Willey, R., Rabson, A., and Martin, M. A. (1986) Production of Acquired Immunodeficiency Syndrome-Associated Retrovirus in Human and Nonhuman Cells Transfected with an Infectious Molecular Clone. *J. Virol. 59*, 284–291.
43. Ono, A., and Freed, E. O. (2004) Cell-Type-Dependent Tageting of Human Immunodeficiency Virus Type 1 Assembly to the Plasma Membrane and the Multivesicular body. *J. Virol. 78*, 1552–1563.
44. Ono, A., Demirov, D., and Freed, E. O. (2000) Relationship between human immunodeficiency virus Type-1 Gag multimerization and membrane binding. *J. Virol. 74*, 5142–5150.
45. Ono, A., and Freed, E. O. (1999) Binding of Human Immunodeficiency Virus Type 1 gag to membrane: Role of the matrix amino terminus. *J. Virol. 73*, 4136–4144.
46. Saad, J. S., Kim, A., Ghanam, R. H., Dalton, A. K., Vogt, M. V., Wu, Z., Lu, W., and Summers, M. F. (2007) Mutations that mimic phosphorylation of the HIV-1 matrix protein do not perturb the myristyl switch. *Protein Sci. 16*, 1793–1797.
47. Briggs, J. A. G., Riches, J. D., Glass, B., Bartonova, V., Zanetti, G., and Kräusslich, H.-G. (2009) Structure and assembly of immature HIV. *Proc. Natl. Acad. Sci. U.S.A. 106*, 11090–11095.
48. Ganser-Pornillos, B. K., Cheng, A., and Yeager, M. (2007) Structure of full-length HIV-1 CA: A model for the mature capsid lattice. *Cell 131*, 70–79.
49. Hogue, I. B., Hoppe, A., and Ono, A. (2009) Quantitative FRET Microscopy Analysis of HIV-1 Gag-Gag Interaction: The Relative Contributions of CA and NC Domains, and Membrane Binding. *J. Virol. 83*, 7322–7336.
50. Joshi, A., Nagashima, K., and Freed, E. O. (2006) Mutation of dileucine-like motifs in the human immunodeficiency virus type 1 capsid disrupts virus assembly, gag-gag interactions, gag-membrane binding, and virion maturation. *J. Virol. 80*, 7939–7951.
51. Li, S., Hill, C. P., Sundquist, W. I., and Finch, J. T. (2000) Image reconstructions of helical assemblies of the HIV-1 CA protein. *Nature 407*, 409–413.
52. Wright, E. R., Schooler, J. B., Ding, H. J., Kieffer, C., Fillmore, C., Sundquist, W. I., and Jensen, G. J. (2007) Electron crytomography of immature HIV-1 virions reveals the structure of the CA and SP1 Gag shells. *EMBO J. 26*, 2218–2226.
53. Gamble, T. R., Yoo, S., Vajdos, F. F., von Schwedler, U. K., Korthylake, D. K., Wang, H., McCutcheon, J. P., Sundquist, W. I., and Hill, C. P. (1997) Structure of the carboxyl-terminal dimerization domain of the HIV-1 capsid protein. *Science 278*, 849–853.
54. Yoo, S., Myszka, D. G., Yeh, C., McMurray, M., Hill, C. P., and Sundquist, W. I. (1997) Molecular recognition in the HIV-1 capsid/cyclophilin A complex. *J. Mol. Biol. 269*, 780–795.
55. Datta, S. A. K., Zhao, Z., Clark, P. K., Tarasov, S., Alexandratos, J. N., Campbell, S. J., Kvaratskhelia, M., Lebowitz, J., and Rein, A. (2007) Interactions between HIV-1 Gag Molecules in Solution: An Inositol Phosphate-mediated Switch. *J. Mol. Biol. 365*, 799–811.
56. Kumar, S., and Nussinov, R. (1999) Salt Bridge Stability in Monomeric Proteins. *J. Mol. Biol. 293*, 1241–1255.
57. Kumar, S., and Nussinov, R. (2002) Relationship between Ion Pair Geometries and Electrostatic Strengths in Proteins. *Biophys. J. 83*, 1595–1612.
58. Barlow, D. J., and Thornton, J. M. (1983) Ion-pairs in Proteins. *J. Mol. Biol. 168*, 867–885.
59. Hill, C. P., Worthylake, D., Bancroft, D. P., Christensen, A. M., and Sundquist, W. I. (1996) Crystal Structures of the Trimeric HIV-1 Matrix Protein: Implications for Membrane Association. *Proc. Natl. Acad. Sci. U.S.A. 93*, 3099–3104.
60. Pelchen-Matthews, A., Krameer, B., and Marsh, M. (2003) Infectious HIV-1 assembles in late endosomes in primary macrophages. *J. Cell Biol. 162*, 443–445.
61. Garcia, E., Pion, M., Pelchen-Matthews, A., Collinson, L., Arrighi, J. F., Blot, G., Leuba, F., Escola, J. M., Demaurex, N., Marsh, M., and Piguet, V. (2005) HIV-1 trafficking to the dendritic cell-T-cell infectious synapse uses a pathway of tetraspanin sorting to the immunological synapse. *Traffic 6*, 488–501.
62. Lindwasser, O. W., and Resh, M. D. (2001) Multimerization of human immunodeficiency virus type 1 Gag promotes its localization to barges, raft-like membrane microdomains. *J. Virol. 75*, 7913–7924.
63. Burniston, M. T., Cimarelli, A., Colgan, J., Curtis, S. P., and Luba, J. (1999) Human immunodeficiency virus type 1 Gag polyprotein multimerization requires the nucleocapsid domain and RNA and is promoted by the capsid-dimer interface and the basic region of matrix protein. *J. Virol. 73*, 8527–8540.
64. Dou, J., Wang, J.-J., Chen, X., Li, H., Ding, L., and Spearman, P. (2009) Characterization of a myristoylated, monomeric HIV Gag protein. *Virology 387*, 341–352.
65. Morikawa, Y., Hockley, D. J., Nermut, M. v., and Jones, I. M. (2000) Roles of matrix, p2, and N-terminal myristoylation in Human Immunodeficiency Virus Type 1 Gag assembly. *J. Virol. 74*, 16–23.
66. Morikawa, Y., Zhang, W.-H., Hockley, D. J., Nermut, M. V., and Jones, I. M. (1998) Detection of a Trimeric Human Immunodeficiency Virus Type 1 Gag Intermediate Is Dependent on Sequences in the Matrix Protein, p17. *J. Virol. 72*, 7659–7663.
67. Dalton, A. K., Ako-Adjei, D., Murray, P. S., Murray, D., and Vogt, M. V. (2007) Electrostatic Interactions Drive Membrane Association of the Human Immunodeficiency Virus Type 1 Gag MA Domain. *J. Virol. 81*, 6434–6445.
68. Alfadhli, A., Huseby, D., Kapit, E., Colman, D., and Barklis, E. (2007) Human Immunodeficiency Virus Type 1 Matrix Protein Assembles on Membranes as a Hexamer. *J. Virol. 81*, 1472–1478.
69. Cimarelli, A., Sandin, S., Hoglund, S., and Luban, J. (2000) Basic residues in human immunodeficiency virus type 1 nucleocapsid promote virion assembly via interaction with RNA. *J. Virol. 74*, 3046–3057.
70. Dawson, L., and Yu, X. F. (1998) The role of nucleocapsid of HIV-1 in virus assembly. *Virology 251*, 141–157.
71. Muriaux, D., Mirro, J., Harvin, D., and Rein, A. (2001) RNA is a structural element in retrovirus particles. *Proc. Natl. Acad. Sci. U.S.A. 98*, 5246–5251.
72. Alfadhli, A., Barklis, R. L., and Barklis, E. (2009) HIV-1 matrix organizes as a hexamer of trimers on membranes containing phosphatidylinositol-(4,5)-bisphosphate. *Virology 387*, 466–472.
73. Franke, E. K., Yuan, H. E. H., Bossolt, K. L., Goff, S. P., and Luban, J. (1994) Specificity and sequence requirements for interactions between various retroviral Gag proteins. *J. Virol. 68*, 5300–5305.
74. Hamard-Peron, E., Juilliard, F., Saad, J. S., Roy, C., Roingeard, P., Summers, M. F., Darlix, J. L., Picart, C., and Muriaux, D. (2010) Targeting of MuLV Gag to the plasma membrane is mediated by PI(4,5)P2/PS and a polybasic region in the Matrix. *J. Virol. 84*, 503–515.
75. Chan, R., Uchil, P. D., Jin, J., Shui, G., Ott, D. E., Mothes, W., and Wenk, M. R. (2008) Retroviruses Human Immunodeficiency Virus and Murine Leukemia Virus Are Enriched in Phosphoinositides. *J. Virol. 82*, 11228–11238.
76. Alfadhli, A., Still, A., and Barklis, E. (2009) Analysis of Human Immunodeficiency Virus Type 1 Matrix Binding to Membranes and Nucleic Acids. *J. Virol. 83*, 12196–12203.
77. Campbell, S., and Vogt, V. M. (1995) Self-assembly *in vitro* of of purifyed CA-NC proteins from Rous sarcoma virus and human immunodeficiency virus type 1. *J. Virol. 69*, 6487–6497.
78. Ehrlich, L. S., Fong, S., Scarlata, S., Zybarth, G., and Carter, C. (1996) Partitioning of HIV-1 gag and gag-related proteins to membranes. *Biochemistry 35*, 3933–3943.
79. Ono, A., Huang, M., and Freed, E. O. (1997) Characterization of human immunodeficiency virus type 1 matrix revertants: Effects on virus assembly, Gag processing, and Env incorporation into virions. *J. Virol. 71*, 4409–4418.
80. Paillart, J.-C., and Gottlinger, H. G. (1999) Opposing effects of human immunodeficiency virus type 1 matrix mutations support a myristyl switch model of Gag membrane targeting. *J. Virol. 73*, 2604–2612.
81. Conte, M. R., Klikova, M., Hunter, E., Ruml, T., and Matthews, S. (1997) The three-dimensional solution structure of the matrix protein from the type D retrovirus, the Mason-Pfizer monkey virus, and implications for the morphology of retroviral assembly. *EMBO J. 16*, 5819–5826.

82. Hatanaka, H., Iourin, O., Rao, Z., Fry, E., Kingsman, A., and Stuart, D. I. (2002) Structure of the Equine Infectious Anemia Virus Matrix Protein. *J. Virol. 76*, 1876–1883.
83. Christensen, A. M., Massiah, M. A., Turner, B. G., Sundquist, W. I., and Summers, M. F. (1996) Three-dimensional structure of the HTLV-II matrix protein and comparative analysis of matrix proteins from the different classes of pathogenic human retroviruses. *J. Mol. Biol. 264*, 1117–1131.
84. McDonnell, J. M., Fushman, D., Cahill, S. M., Zhou, W., Wolven, A., Wilson, C. B., Nelle, T. D., Resh, M. D., Wills, J., and Cowburn, D. (1998) Solution structure and dynamics of the bioactive retroviral M domain from Rous sarcoma virus. *J. Mol. Biol. 279*, 921–928.
85. Riffel, N., Harlos, K., Lourin, O., Rao, Z., Kingsman, A., Stuart, D., and Fry, E. (2002) Atomic Resolution Structure of Moloney Leukemia virus Matrix protein and Its Relationship to Other Retroviral Matrix Proteins. *Structure 10*, 1627–1636.
86. Matthews, S., Mikhailov, M., Burny, A., and Roy, P. (1996) The solution structure of the bovine leukemia virus matrix protein and similarity with lentiviral matrix proteins. *EMBO J. 15*, 3267–3274.
87. Takayama, Y., Castaeda, C. A., Chimenti, M., Garca-Moreno, B., and Iwahara, J. (2008) Direct Evidence for Deprotonation of a Lysine Side Chain Buried in the Hydrophobic Core of a Protein. *J. Am. Chem. Soc. 130*, 6714–6715.
88. Gottlieb, R. A., Giesing, H. A., Zhu, J. Y., Engler, R. L., and Babior, B. M. (1995) Cell acidification in apoptosis: Granulocyte colony-stimulating factor delays programmed cell death in neutrophils by up-regulating the vacuolar H(+)-ATPase. *Proc. Natl. Acad. Sci. U.S.A. 92*, 5965–5968.
89. Moolenaar, W. H., Tsien, R. Y., van der Saag, P. T., and de Laat, S. W. (1983) Na^+/H^+ exchange and cytoplasmic pH in the action of growth factors in human fibroblasts. *Nature 304*, 645–648.
90. Schuldiner, S., and Rozengurt, E. (1982) Na^+/H^+ antiport in Swiss 3T3 cells: Mitogenic stimulation leads to cytoplasmic alkalinization. *Proc. Natl. Acad. Sci. U.S.A. 79*, 7778–7782.
91. Makutonina, A., Voss, T. G., Plymale, D. R., Fermin, C. D., Norris, C. H., Vigh, S., and Garry, R. F. (1996) Human immunodeficiency virus infection of T-lymphoblastoid cells reduces intracellular pH. *J. Virol. 70*, 7049–7055.